Adsorption of Organic Dyes by Fe_3O_4@C, Fe_3O_4@C@C, and Fe_3O_4@SiO_2 Magnetic Nanoparticles

O. S. Ivanova[a, b, *], **I. S. Edelman**[a], **A. E. Sokolov**[a, b], **E. S. Svetlitsky**[a], **S. M. Zharkov**[a, b], **A. L. Sukhachev**[a], **Ch. R. Lin**[c], **and Yu. Zh. Chen**[c]

[a] *Kirensky Institute of Physics, Siberian Branch, Russian Academy of Sciences, Krasnoyarsk, 660036 Russia*
[b] *Siberian Federal University, Krasnoyarsk, 660041 Russia*
[c] *National Pingtung University, Pingtung, 900392 Taiwan*
*e-mail: osi@iph.krasn.ru

Abstract—Fe_3O_4@C, Fe_3O_4@C@C, and Fe_3O_4@SiO_2 core–shell nanoparticles are synthesized via thermal decomposition and coprecipitation. Samples are characterized via X-ray spectroscopy, transmission electron microscopy, and magnetometry. It is shown that the magnetic core of all nanoparticles is nanocrystalline and has crystal parameters corresponding to only one phase of Fe_3O_4, covered with a uniform shell of amorphous carbon or silicon oxide around 8 nm thick. Special attention is given to adsorption properties of the nanoparticles with respect to four dyes: Methylene blue, Congo Red, Eosin Y, and Rhodamine C. The high selectivity of Fe_3O_4@C nanoparticles to various dyes is revealed.

INTRODUCTION

Magnetic nanomaterials characterized by exceptional morphological, physical, and chemical properties are indispensable when seeking new solutions to technological problems in almost every sphere of human activity. One threat to mankind is the deteriorating quality of water and its contamination with numerous manufacturing wastes. Dyes, heavy-metal impurities, and pathogenic bacteria constitute the bulk of substances polluting our water ecosystem. Laboratories around the world are working to create ever more efficient and cost-effective materials for water purification that can withstand many cycles. Thanks to such advantages as simplicity of functionalization, chemical stability, and magnetic properties, magnetic nanoparticles (NPs) are a leading candidate for the removal of polluting elements like heavy metals [1–3], pharmaceuticals [4–6], and different dyes [7–10] from aqueous solutions. Synthetic dyes are the main group of chemicals contaminating our water ecosystem. They are contained in the waste water of textile, leather, cosmetic, paper, and other industries. Dyes are divided into three classes: anionic (acid), cationic (basic), and neutral (mixtures of acid and base dyes). As stable organic chemicals with good solubility, dyes are particularly hazardous to aquatic organisms. Standard waste treatment facilities are inefficient in removing soluble dyes, resulting in contamination of watercourses and deterioration of the environment [11]. Substantial benefits of purifying adsorption waste water using NPs is simplicity of the magnetic withdrawal of particles and the regeneration of adsorption capacity via the desorption of contaminants adsorbed on their surfaces. Adsorption of a dye is the outcome of two mechanisms (adsorption and ion exchange) and depends on many factors, including dye/adsorbent interaction, adsorbent surface area, particle size, temperature, pH, and period of contact. Selective adsorption of certain contaminants can be achieved by modifying the surfaces of NPs and creating magnetic core–functional shell structures. Covering the NP surfaces with different coatings also increases their resistance to aggregation and precludes interparticle interaction. An investigation of the current literature and the real demand for water purification shows the need for rapid progress in this area. The challenge is that NPs designed for these purposes must have both high adsorption capacity and the magnetic properties required for successfully removing them from purified water (i.e., fairly strong magnetization and a conversely weak coercive force). The importance of searching for increasingly better combinations of these properties can thus not be overemphasized.

This work was devoted to a comparative investigation of the adsorption of organic dyes—cationic (Methylene Blue (MB), Rhodamine C (RhC)) and anionic (Congo Red (CR), Eosin Y (EoY))—by Fe_3O_4 magnetite nanoparticles covered with different shells: C, C@C, and SiO_2.

SYNTHESIS AND CHARACTERIZATION OF NANOPARTICLES

Initial magnetite NPs for the Fe_3O_4@C structure were obtained via thermal decomposition. An iron–oleate complex was first synthesized through 4 h of the decomposition of sodium oleate and iron chloride hexahydrate $FeCl_3 \cdot 6H_2O$, dissolved in a mixture of alcohol, deionized water, and *n*-hexane, in air at 70°C. The resulting iron–oleate complex was then blended with oleic acid (OA), dissolved in 1-octadecene (ODE), held in air for 3 h at 320°C, and cooled to room temperature. After it cooled, 500 mL of ethanol was added, the lower layer was removed, and *n*-hexane was added. A black residue formed that was a mixture of Fe_3O_4 nanoparticles and residual products of the products reaction. The nanoparticles were separated using a magnetic field, washed several times with *n*-hexane, and dried for 6 h at 30°C.

To obtain Fe_3O_4@C, a mixture of Fe_3O_4 NPs with glucose was dispersed in distilled water for 15 min in an ultrasonic bath, mixed for 30 min, and sealed in an autoclave of stainless steel coated with Teflon. The autoclave was heated to 200°C, held at this temperature for 12 h, and cooled to room temperature under ambient conditions. The resulting product was separated using a magnetic field, washed several times in water and ethanol, and dried for 6 h at 60°C.

To synthesize NPs with a double carbon shell, Fe_3O_4@C NPs obtained in a one-stage process of thermal decomposition of a mixture of iron nitrate nonahydrate, $Fe(NO_3)_3 \cdot 9H_2O$, oleic acid, and oleylamine [12], were employed as initial particles. The final NPs were coated with a second carbon shell in glucose dissolved in distilled water, as was described above.

Fe_3O_4@SiO_2 NPs were obtained in a two-stage process [13]. Fe_3O_4 NPs were first synthesized via co-deposition using iron sulfide $FeSO_4 \cdot 7H_2O$, KNO_3, and NaOH. Mixing was done in an argon flow for 1 h at 90°C with ethanol washing. The magnetite NPs were covered with silicon oxide according to Stöber [14]. Fe_3O_4 NPs were dispersed in ethanol and kept in a water bath for 15 min with ultrasonication. The suspension of NPs was then supplemented slowly with a solution of ammonium and tetraethoxysilane $Si(OC_2H_5)_4$ (TEOS). The resulting Fe_3O_4@SiO_2 NPs were collected with a permanent NdFeB magnet and washed in ethanol. The investigated NPs thus differed by both the type of the nonmagnetic shell and the means of synthesis.

The crystal structure of the obtained NPs was studied via X-ray diffraction on an XRD 6000 diffractometer (Shimadzu) using CuK_α radiation with a wavelength of 1.54056 Å. Morphology was investigated via transmission electron microscopy (TEM) on a JEM-2100 microscope at an accelerating voltage of 200 kV. Dependences of the magnetization of NPs on an external magnetic field were recorded using a VSM 8604

(LakeShore Cryotronics) vibration magnetometer. Absorption spectra of dye solutions were investigated in a quartz cell with an optical path length of 5 mm on a UV/VIS SKD-2MUF circular dichroism spectrometer (Department of Laser–Spectral Instrumentation, Institute of Spectroscopy, Russian Academy of Sciences, Moscow).

To investigate the adsorption capacity of NPs, they were dispersed for 10 min in an aqueous dye solution of a certain concentration in an ultrasonic bath. The NPs were then removed from the solution using a magnetic field, and the optical absorption of the solution was measured at wavelengths corresponding to the dyes' maxima of absorption: 490 nm for EoY, 505 nm for CR, 664 nm for MB, and 550 nm for RhC. The proportion of the dye adsorbed by nanoparticles during their interaction with it was calculated from the change in absorption relative to that of the initial solution. Calibration curves for the dependence of the intensity of the absorption signal on dye concentration were recorded in advance for each dye. The residual solution was mixed again with magnetic particles, and the procedure was repeated until the solution became transparent. Adsorption capacity q_t (mg/g) of the NPs was determined using the formula

$$q_t = \frac{(C_0 - C_t)V}{m}, \tag{1}$$

where C_0 and C_t are the initial and current (measured at any time) dye concentrations of the solution, V is the volume of the solution, and m is the mass of NPs introduced into the solution. The time dependence of q_t, referred to as a kinetic curve, is the most important characteristic of the efficiency of an adsorbent. The dependences of equilibrium adsorption capacity q_e on the concentration of the dye in a solution and the adsorption isotherm were measured for each dye in a wide range of concentrations under conditions where equilibrium was reached.

RESULTS AND DISCUSSION

X-ray diffraction patterns of the studied NPs shown in Fig. 1 show that the cores of all particles had a spinel crystal structure with lattice parameters corresponding to the Fe_3O_4 phase, since all main reflections were those of the reference data for this phase (PDF Card no. 04-002-3668).

Images obtained on an electron microscope (TEM images) revealed that when using iron chloride and nitrate hydrates in synthesizing the initial NPs, they grew mostly in the shape of smoothed hexagons or spheres (Figs. 2a and 2b). With iron sulfide, they grew in a shape close to rectangular (Fig. 2c) (i.e., the nanoparticles grew in different crystallographic planes). In all cases, however, the average particle size was 40 to 50 nm. In the structure with a double carbon shell, isolated NPs and conglomerates of them formed
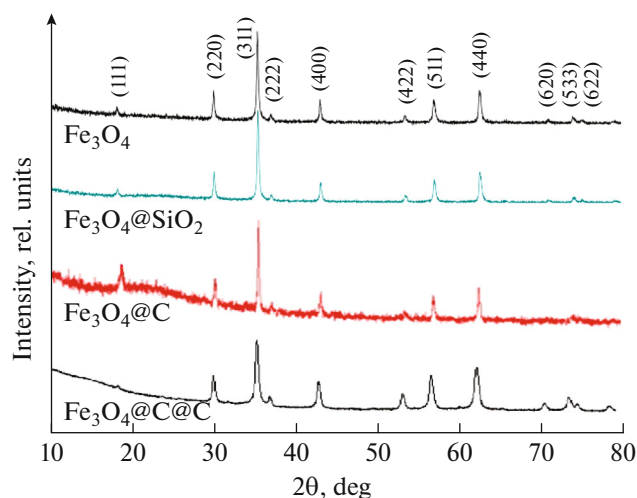
Fig. 1. Diffraction patterns of NPs. Indices of characteristic Fe_3O_4 magnetite reflections (PDF Card no. 04-002-3668) are indicated above the upper curve for Fe_3O_4 NPs.

with sizes up to 200 nm. An amorphous shell around 8 nm thick is clearly seen in Figs. 2a and 2c.

The saturation magnetization for magnetite NPs of 70 to 75 CGS-ESU system units/g was close to that of bulk magnetite of 84 CGS-ESU system units/g [15] and 55 to 65 CGS-ESU system/g for shelled NPs (Fig. 3). The small drop in magnetization for core–shell NPs can be explained by the overall mass of the nanoparticles including a fraction of the mass of the coating material, which was not considered in determining the magnetization. In all cases, the coercive force did not exceed 140 Oe.

Figure 4 shows kinetic curves of the adsorption of cationic (Fig. 4a) and anionic (Fig. 4b) dyes by NPs coated with different shells. The adsorption kinetic curves for the cationic dye MB are in all cases close to one another. The values and rates of adsorption differ somewhat in the initial regions. Kinetic data of RhC adsorption are also given for the Fe_3O_4@C NPs.

The experimental data were described by fitting with nonlinear adsorption equations [16] of the pseudo-first order

$$q_t = q_e \left(1 - e^{-k_1 t}\right) \tag{2}$$

and the pseudo-second order

$$q_t = \frac{q_e^2 k_2 t}{1 + q_e k_2 t}, \tag{3}$$

where q_e is equilibrium sorption, and k_1 and k_2 are the adsorption rate constants for the pseudo-first and pseudo-second order reactions, respectively.

The kinetic data of MB adsorption by Fe_3O_4@SiO$_2$ and Fe_3O_4@C@C NPs are described well by the pseudo-second order model. The lines in Fig. 4a show the fitting curves that best describe the experimental data. The coefficients of correlation and rate constants determined in fitting are higher in such cases, and adsorption can in these cases be controlled via chemisorption. The adsorption capacity of Fe_3O_4@SiO$_2$ NPs shows comparable adsorption values for the cationic (MB) and anionic (CR) dyes, which can be used in solutions containing complex contaminants. Fe_3O_4@C@C NPs adsorb primarily cationic dyes, but they can also adsorb anionic dyes, albeit with a lower capacity and a slower rate (curve *2* in Fig. 4b). The adsorption capacity of Fe_3O_4@C NPs was selective with respect to cationic dyes, and anionic dyes (CR, EoY, Methyl Orange) are not adsorbed by them at all (curve *1* in Fig. 4b).

Figure 5 shows the low coefficient of adsorption for Fe_3O_4@C@C NPs does not allow a good description of the isotherm throughout the range of concentrations, and the experimental data fit the Langmuir curve only at low concentrations. In all other cases, the concentration dependences of the equilibrium adsorption capacity are closer to the Langmuir equation, evidence of the formation of a uniform adsorption layer of molecules that do not interact with one another.
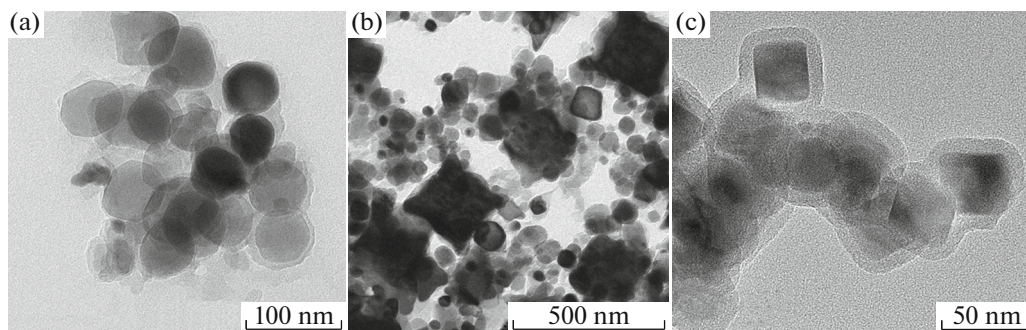

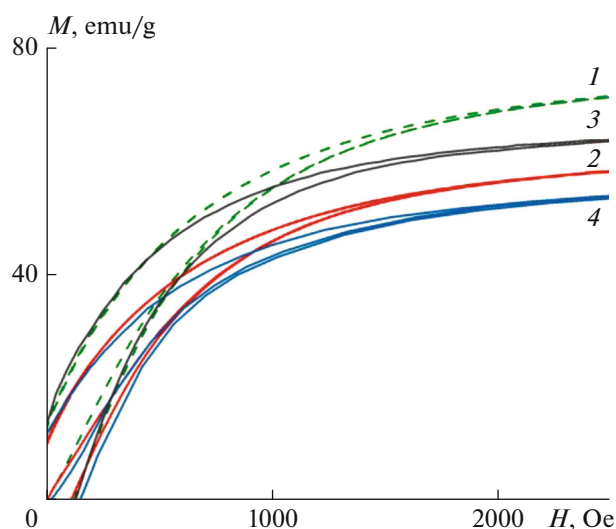**Fig. 2.** TEM images of NPs in the (a, b) Fe_3O_4@C@C and (c) Fe_3O_4@SiO$_2$ samples.

Fig. 3. Field dependences of magnetization of Fe_3O_4, $Fe_3O_4@C$, $Fe_3O_4@C@C$, and $Fe_3O_4@SiO_2$ NPs, curves *1−4*, respectively.
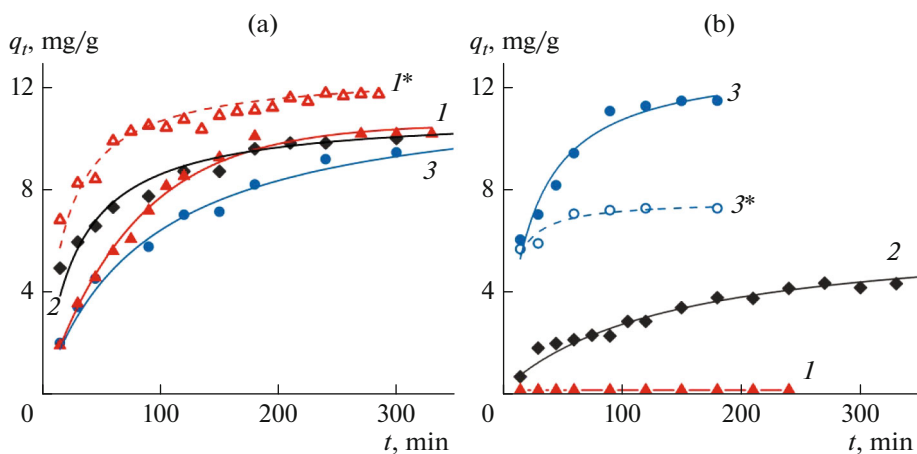

Fig. 4. Kinetic curves of adsorption of (a) cationic dyes (curves *1−3*) MB and (curve *1**) RhC, and (b) anionic dyes (curves *1−3*) CR and (curve *3**) EoY by $Fe_3O_4@C$, $Fe_3O_4@C@C$, and $Fe_3O_4@SiO_2$ nanoparticles (curves *1* and *1**, *2*, *3* and *3**, respectively). Experimental conditions: $C_0 = 30$ mg/L, m(NPs) = 3 mg, $V = 1.5$ mL. Lines show results from fitting the experimental data to the pseudo-second order adsorption model, except for MB adsorption by $Fe_3O_4@C$ NPs, which is fit best by the pseudo-first order model (curve *1*).

CONCLUSIONS

$Fe_3O_4@C$, $Fe_3O_4@C@C$, and $Fe_3O_4@SiO_2$ magnetic core−shell nanoparticles were synthesized by different modifications of thermal decomposition and coprecipitation. Data from X-ray structural analysis and electron microscopy revealed that the magnetic core of nanoparticles had a magnetite Fe_3O_4 crystal structure and contained no other phases. Transmission electron microscopy showed chiefly hexagonal or spherical NPs for synthesis using iron chloride and nitrate hydrates and chiefly rectangular NPs when using iron sulfide as a precursor. The average size of isolated NPs was 50 nm. At the same time, giant con- glomerates of NPs with sizes up to 200 nm formed in the samples covered with double carbon coating. Uniform shells of amorphous carbon or carbon oxide about 8 nm thick formed around the magnetic cores of NPs. Magnetic measurements revealed high saturation magnetization in all samples. This can be considered an advantage of the studied nanomaterials, since higher magnetization requires us to use weaker magnetic fields for controlling processes involving these materials.

The adsorption capacity of the studied NPs and the kinetics of adsorption were investigated with respect to two anionic dyes (Congo Red (CR) and Eosin Y (EoY))
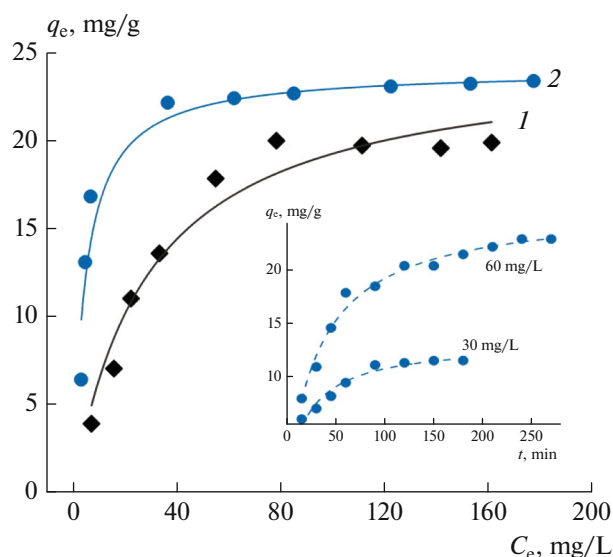
Fig. 5. Isotherm of CR adsorption by (*1*) Fe$_3$O$_4$@C@C and (*2*) Fe$_3$O$_4$@SiO$_2$ nanoparticles. The lines are curves that describe the experimental data according to the Langmuir equation [17] with parameters $k_L = 0.034$ L/mg, $q_{max} = 23.8$ mg/L, and $R^2 = 0.958$ for Fe$_3$O$_4$@C@C nanoparticles, and $k_L = 0.21$ L/mg, $q_{max} = 24$ mg/L, and $R^2 = 0.97$ for Fe$_3$O$_4$@SiO$_2$ nanoparticles. Kinetic curves of adsorption by Fe$_3$O$_4$@SiO$_2$ nanoparticles are shown in the inset for two initial CR concentrations.

and two cationic dyes (Methylene Blue (MB) and Rhodamine C (RhC)). It was shown that the adsorption of these dyes by the studied NPs proceeds according to a pseudo-second-order kinetic model, suggesting that sorption depends on the amount of the dissolved substance adsorbed on the adsorbent's surface and the number of active sites. The high initial rates of adsorption were observed for all dyes, testifying to the rapidness of the initial dye removal and the dominating role of external surface diffusion, particularly for CR adsorption by NPs with a double carbon shell. It was shown that the experimental data agreed with the Langmuir model of adsorption, evidence that homogeneous and single-layer adsorption dominated in the considered cases. The high selectivity of NPs with a single carbon shell toward cationic dyes was revealed. They were characterized by the maximum adsorption capacity with respect to Rhodamine C and adsorb absolutely no Congo Red, Eosin Y, or Methyl Orange. Analysis of the experimental data demonstrates the key role of surface properties of our synthesized NPs in the adsorption of different dyes.

CONFLICT OF INTEREST

The authors declare that they have no conflicts of interest.

REFERENCES

1. Wana, Sh., Yu, Ch., Li, Y., et al., *Chem. Eng. J.*, 2021, vol. 405, p. 126576.

2. Badruddoza, A.Z.M., Shawon, Z.B.Z., Tay, W.J.D., Hidajat, K., et al., *Carbohydr. Res.*, 2013, vol. 91, p. 322.

3. Bharti, M.K., Gupta, S., Chalia, S., et al., *J. Supercond. Novel Magn.*, 2020, vol. 33, p. 3651.

4. Saiz, J., Bringas, E., and Ortiz, I., *J. Chem. Technol. Biotechnol.*, 2014, vol. 89, p. 909.

5. Bao, X., Qiang, Z., Chang, J.H., et al., *J. Environ. Sci.*, 2014, vol. 26, no. 5, p. 962.

6. Chen, L., Liu, Y., He, X., and Zhang, Y., *Chin. J. Chromatogr.*, 2015, vol. 33, no. 5, p. 481.

7. Xiang, H., Ren, G., Zhong, Y., et al., *Nanomaterials*, 2021, vol. 11, p. 330.

8. Xu, P., ZEng., G.M., Huang, D.L., et al., *Sci. Total Environ.*, 2012, vol. 424, p. 1.

9. Allégre, C., Moulin, P., Maisseu, M., et al., *J. Membr. Sci.*, 2006, vol. 269, p. 15.

10. Ghorbani, F. and Kamari, S., *Environ. Technol. Innovation*, 2019, vol. 14, p. 100333.

11. Robinson, T., McMullan, G., Marchant, R., et al., *Bioresour. Technol.*, 2001, vol. 77, p. 247.

12. Lin, Ch.-R., Ivanova, O.S., Edelman, I.S., et al., *Nanomaterials*, 2022, vol. 12, p. 376.

13. Lin, Ch.-R., Ivanova, O.S., Petrov, D.A., et al., *Nanomaterials*, 2021, vol. 11, p. 2371.

14. Stöber, W., Fink, A., and Bohn, E., *J. Colloid Interface Sci.*, 1968, vol. 26, p. 62.

15. Smit, J. and Wijn, H.P.J., *Ferrites: Physical Properties of Ferrimagnetic Oxides in Relation to Their Technical Applications*, Eindhoven: N.V. Philips, 1959.

16. Azizian, S., *J. Colloid Interface Sci.*, 2004, vol. 276, p. 47.

17. Langmuir, I., *J. Am. Chem. Soc.*, 1918, vol. 40, p. 1361.

Translated by Z. Smirnova